JOURNAL OF GEOPHYSICAL RESEARCH, VOL. 99, NO. A4, PAGES 6543–6552, APRIL 1, 1994

Speeds of coronal mass ejections: SMM observations from 1980 and 1984–1989

A. J. Hundhausen, J. T. Burkepile, and O. C. St. Cyr[1]

High Altitude Observatory, National Center for Atmospheric Research, Boulder, Colorado

Abstract. The speeds of 936 features in 673 coronal mass ejections have been determined from trajectories observed with the Solar Maximum Mission (SMM) coronagraph in 1980 and 1984–1989. The distribution of observed speeds has a range (from 5th to 95th percentile) of 35 to 911 km s^{-1}; the average and median speeds are 349 and 285 km s^{-1}. The speed distributions of some selected classes of mass ejections are significantly different. For example, the speeds of 331 "outer loops" range from 80 to 1042 km s^{-1}; the average and median speeds for this class of ejections are 445 and 372 km s^{-1}. The speed distributions from each year of SMM observations show significant changes, with the annual average speeds varying from 157 (1984) to 458 km s^{-1} (1985). These variations are not simply related to the solar activity cycle; the annual averages from years near the sunspot maxima and minimum are not significantly different. The widths, latitudes, and speeds of mass ejections determined from the SMM observations are only weakly correlated. In particular, mass ejection speeds vary only slightly with the heliographic latitudes of the ejection. High-latitude ejections, which occur well poleward of the active latitudes, have speeds similar to active latitude ejections.

1. Introduction

The data set obtained with the coronagraph/polarimeter flown on the Solar Maximum Mission (SMM) spacecraft has proven a major store of information on the phenomenon of coronal mass ejections. Operation of this instrument in 1980 and from 1984 through 1989 led to observation of 1351 mass ejections over most of a sunspot cycle. The SMM observations are thus particularly well-suited to statistical analysis of mass ejection properties and the search for systematic changes in those properties on the timescale of a solar activity (or sunspot) cycle. The goal of such an analysis is to sharpen our understanding of mass ejections per se, of the relationship to other forms of solar activity, and of the physical origins of the mass ejection phenomenon (see the review papers referenced by *Hundhausen* [1993]).

Recently, *Hundhausen* [1993] provided a statistical analysis of the sizes and locations of the mass ejections observed with the SMM instrument. This paper will continue along a similar path with a statistical analysis of another important property of mass ejections, the speeds at which they leave the solar corona. We will summarize the 936 measurements of mass ejection speeds tabulated by *Burkepile and St. Cyr* [1993] and examine evidence for systematic variations over the 10-year epoch of SMM observations. We will also look for any relationships among the three mass ejection properties that have been extensively measured and tabulated using the SMM data set, namely, the sizes and locations (as described by *Hundhausen* [1993]) and the speeds described here.

[1]Now at AlliedSignal Technical Services Corporation, NASA Goddard Space Flight Center, Greenbelt, Maryland.

Paper number 93JA03586.
0148-0227/94/93JA-03586$05.00

2. Definitions and Measurements

The definition of a coronal mass ejection used in examination of the SMM data set remains that given by *Hundhausen et al.* [1984 p. 2639] and *Hundhausen* [1993 p. 13,177]; i.e., " . . . an observable change in corona structure that (1) occurs on a time scale between a few minutes and several hours and (2) involves the appearance of a new discrete, bright white-light feature in the coronagraph field of view." *Burkepile and St. Cyr* [1993] have added speed measurements and a uniform description of mass ejection morphologies to the information in the earlier catalog of *St. Cyr and Burkepile* [1990]. These additions required a reexamination of all mass ejections observed by SMM and led to minor changes in the number of identified ejections and in a few measured values of angular widths and locations. All quantities used in this paper are from the 1993 tabulation.

The motion of any sufficiently distinct or sharp feature in a mass ejection can be quantified if the feature is visible on a succession of images. Our interest here is in the departure of the feature from the Sun, or in its motion in the direction radial from the Sun. The determination of this motion and its characterization in terms of an "apparent speed" are similar to that used in earlier Skylab and Solwind studies; it has been described in detail by *Burkepile and St. Cyr* [1993] and will only be outlined here.

The first step in this process is the measurement of the heliocentric position, r, of a mass ejection feature on a time sequence of SMM coronal images. These measurements were usually made at a given position angle (chosen to be as close to the center of the feature as practical) around the solar limb. In a minority of cases the heliocentric position was measured at a changing set of angles because the motion of the feature was significantly nonradial or because its motion carried it across defects in the images or along the boundary of the different sectors around the Sun covered by

successive images. In any case, the resulting set of radial positions $r(t_1)$, $r(t_2)$, $r(t_3)$, $\cdots$ $r(t_n)$ measured at times t_1, t_2, t_3, $\cdots$ t_n give a trajectory for the radial (or nearly radial) motion of the feature within the 1.6 to 4–6 solar radii range of heliocentric distance included in the field of view of the SMM instrument.

A least squares fit of the linear function $r = r_0 + v_1 t$ to each observed trajectory yields a value v_1 that is the average speed during the time interval t_1 to t_n of observation. This is our best determination of an ejection speed for most mass ejection features observed with the SMM instrument. However, there are a significant number of ejections for which the observed trajectory suggests acceleration of a feature within the SMM field of view. In such cases, v_1 is an underestimate of the speed at which the feature was moving when last observed. Thus a least squares fit of a quadratic function $r = r_0 + (a/2)(t - t_0)^2$ was performed for all trajectories with three or more position measurements (or $n \geq 3$). Then $v_2 = a(t_n - t_0)$ is an estimate of the ejection speed at the time t_n when the feature was last observed. In these expressions, r_0 is the location from which the feature starts from rest ($v_2 = 0$) at $t = t_0$. The parameters r_0 and t_0 need not (and usually do not) correspond to any of the observed positions $r(t_i)$ where i ranges from 1 to n. This v_2 has been used as the ejection speed for those features where all of three criteria are met: the spacing of t_1, t_2, t_3, $\cdots$ t_n is adequate to define a nonlinear trajectory; the quadratic function is clearly a better fit to the observed trajectory, with consideration of the uncertainties in the observed $r(t_i)$; and the difference between v_1 and v_2 is significant. For some mass ejection features the trajectory suggests a slow initial motion and then the onset of an acceleration within the SMM field of view (i.e., $t_1 < t_0 < t_n$). In such cases the least squares fit is applied to the observed $r(t_i)$ excluding the values before the onset of acceleration (or for $t_i < t_0$). The reader is again referred to *Burkepile and St. Cyr* [1993] for details. The uncertainties in the final v_1 or v_2 selected as the expansion speed are highly variable. Burkepile and St. Cyr estimate a relative uncertainty of 20% for a speed determination of typical quality.

The radiation recorded in an SMM image is photospheric light that has been scattered by electrons along a line of sight through the optically thin corona. Features that are not centered over the limb of the Sun are then seen projected onto an image plane that is perpendicular to the line of sight. The appendix illustrates this projection for a rising spherical region of dense coronal plasma, a simple but reasonable model for the many mass ejections that appear as a bright loop, mound, or cloud in the SMM data set. This model suggests that the rate of radial motion inferred from a sequence of images is between the true radial speed v (as would be observed if the bubble were actually centered over the solar limb) and the simple trigonometric projection $v \cos \theta$ (where θ is the angle off the limb). This ambiguity will be avoided here by referring to the measured expansion speeds as "apparent speeds." *Hundhausen* [1993] argued that most mass ejections are observed within about 35° of the solar limb. For $\theta \lesssim 35°$, the apparent speeds underestimate the true expansion speeds by a factor less than $1 - \cos 35° = 18\%$.

3. Mass Ejection Speeds

The technique outlined above was successfully applied to 673 of the mass ejections identified in the SMM data set. In some of these mass ejections, trajectories could be measured for more than one distinct feature. For example, a "three-part" structure with an outer bright loop, darker cavity, and interior "core" were often seen among the SMM mass ejections. In a few examples, "multiple parts" (usually distinct loops or clouds) were seen to emerge in quick succession from the same location in the corona. Trajectories for such distinct features within a single mass ejection have been included in this analysis (but not multiple measurements for single features); thus a total of 936 speeds have been determined. In 244 of these cases, only two heliocentric position measurements were possible, and a single value v_1 of the apparent speed was determined by fitting a linear function to these measurements. In 692 of the cases, three or more position measurements were possible, and both a v_1 and v_2 were determined by fitting both linear and quadratic functions to the measured trajectory. In 144 of these cases (or 21%), the quadratic fit was judged to be justified by the data, clearly preferable, and significantly different from the first-order fit, and v_2 was taken as the apparent speed of the feature; the acceleration a was positive for 95% of these cases. In the remaining 548 of these cases (or 79%), v_1 was taken as the apparent speed. For the record, failure to determine the speed of any feature in 678 of the observed mass ejections stemmed from the absence of any sufficiently sharp or distinct feature in 531 cases, from the visibility of features on only a single image in 114 cases, or visibility on several images too close in time to define motion in 33 cases.

All of the speeds determined from SMM observations pertain to an instrumental field of view extending from 1.6 to 4–6 solar radii from Sun center (depending upon location in the square field of view) in heliocentric distance. For the 144 mass ejection features where the quadratic fit to the measured trajectory was judged to be superior, a different final speed would have been deduced from observations in a different field of view. Even for the 792 mass ejection features where the quadratic fit was not possible or clearly preferable, acceleration must have occurred as the mass ejection formed below the field of view of the SMM instrument. Thus observations of the same feature in a different field of view would likely have yielded different values of the apparent speed.

Results

The lowest of the 936 apparent speeds was 7 km s^{-1}, while the highest was (taking the values literally) 2101 km s^{-1}. The distribution of observed values is shown in Figure 1 (with all 18 speeds above 1200 km s^{-1} grouped in the uppermost interval). The statistical range of speeds defined by the 5th and 95th percentiles of the observed distribution extends from 35 to 911 km s^{-1}. The frequency of the observed values falls rather slowly with increasing speed up to 400 km s^{-1}, falls off more rapidly above 400 km s^{-1}, but has an extended tail at speeds above ~800 km s^{-1}. The average apparent speed is 349 km s^{-1}, while the median speed is 285 km s^{-1}. These statistical parameters of the observed speed distribution are summarized in Table 1.

Inclusion of the apparent speeds for several distinct features in some observed mass ejections might be a cause for some

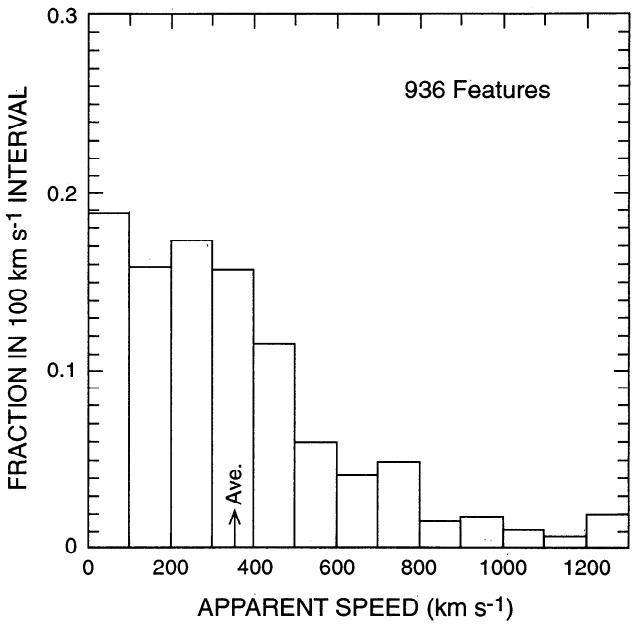

Figure 1. The distribution of apparent speeds for all 936 mass ejection features. All 18 values above 1200 km s^{-1} have been grouped in the highest interval.

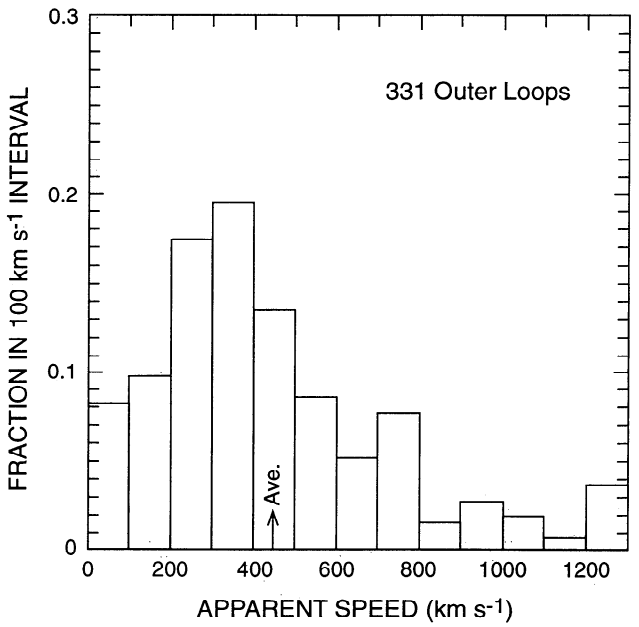

Figure 2. The distribution of apparent speeds for 331 mass ejection "outer loops." All 13 values above 1200 km s^{-1} have been grouped in the highest interval.

concern in interpreting the distribution of values in Figure 1. This concern is alleviated by considering the apparent speed distributions for two subsets of the 936 measurements.

1. There are 698 "outermost features." The outermost feature of a mass ejection has been defined to be the first feature for which the speed of the leading edge can be measured. There is such a feature in each of the 673 ejections under discussion. In ejections with distinct "multiple parts," there can be two (in 23 cases) or three (in a single case) outermost features.

2. There are 627 "primary features." The primary feature of a mass ejection has been defined to be the most important or conspicuous feature. In 65 of the 673 ejections under discussion, the speed of the primary feature could not be measured. There were 19 multiple-part ejections in which there were multiple primary features.

The speed distribution for these features differ only slightly from that in Figure 1. The ranges, average, and median speed for these more restricted subclasses of measured values are also given in Table 1. They are very close to the same statistical parameters for all observed features.

There are, however, some classes of mass ejection features with speed distributions that do differ significantly from the distribution for all features. The most important such class is probably that of bright "looplike" structures that are the outermost or leading feature in many coronal mass ejections. The importance of this class was emphasized in descriptions of the 1973–1974 Skylab coronagraph observations [e.g., *MacQueen*, 1980; *Munro and Sime*, 1985]. Such bright loops were seen in 26% of the mass ejections detected with the Skylab instrument, and it was suggested that this was a particularly simple class of ejections, especially amenable to both empirical and theoretical analysis. In contrast, less than 1% of the mass ejections detected with the Solwind coronagraph in 1979–1981 and 1984–1985 were classified as being "looplike" in appearance [*Howard et al.*, 1985, 1986]. However, the SMM observations revealed a situation more like that from the Skylab era; 47% of the ejections detected with the SMM instrument in 1980 and 1984–1989 contained a bright, looplike feature. Apparent speeds were determined for 331 loops that were the outermost or leading features in mass ejections; the distribution of these speeds is shown in Figure 2. This distribution is distinctly different from that for all features (Figure 1) in the paucity of low values. In fact, the speed distribution for "outer loops" has a distinct peak in the 300 to 400 km s^{-1} interval. The difference is reflected in all statistical parameters: the 5th to 95th percentile range of 80 to 1042 km s^{-1}, the average of 445 km s^{-1}, and the median value of 372 km s^{-1}. These parameters are listed in Table 1.

Table 1. Statistical Parameters of Observed Speed Distributions

	No.	Range, km s^{-1}	Average, km s^{-1}	Median, km s^{-1}	Standard Deviation, km s^{-1}
All features	936	35–911	349	285	289
Outermost features	698	33–911	349	281	298
Primary features	627	31–912	354	291	293
Outer loops	331	80–1042	445	372	315

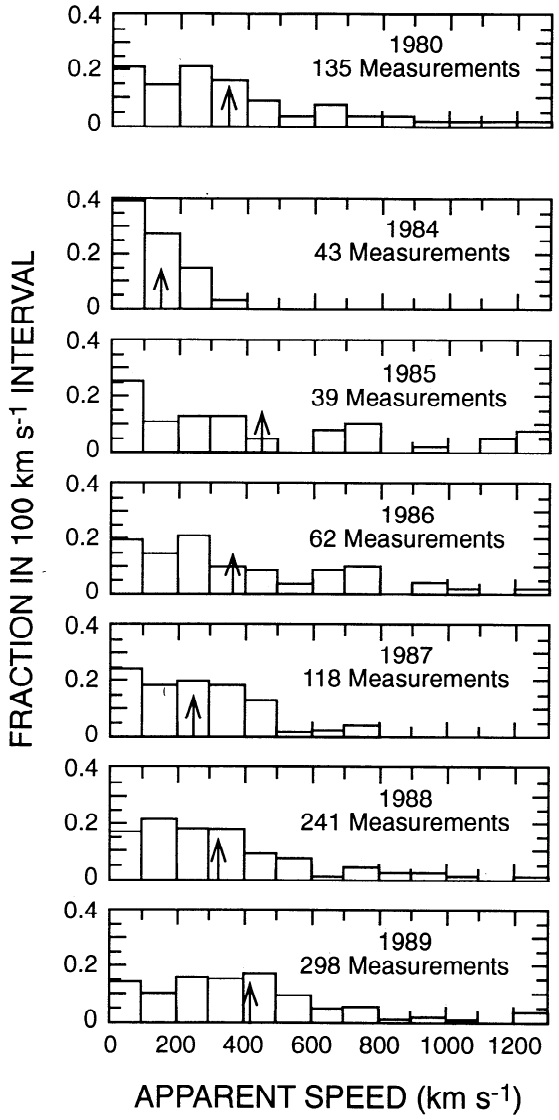

Figure 3. The distributions of apparent speeds (for all mass ejection features) from each calendar year of SMM observations. The average value for each annual distribution is indicated.

The distributions of apparent speeds (for all features) measured during each calendar year of SMM operations are shown in Figure 3. The number of measurements, 5th to 95th percentile range, average speed, and median speed from each year are listed in Table 2. There are rather obvious and distinct differences among these annual distributions and the statistical parameters characterizing them. These differences are epitomized by the distributions and parameters for two consecutive years, 1984 and 1985. The 1984 distribution in Figure 3 shows a rapid decrease in frequency of occurrence for apparent speeds up to 400 km s^{-1}; the highest value measured during 1984 was only 419 km s^{-1}. In contrast, the 1985 distribution in Figure 3 shows apparent speeds spread over the entire range covered in the display; 15 of the measured values (or 38% of the total for the year) are above 400 km s^{-1}. The average of the 43 speed measurements from 1984 is 157 km s^{-1}, the lowest value for any year of SMM observations. The average of the 39 speed measurements

Table 2. Statistical Parameters of the Annual Speed Distributions for All Features

	No.	Range, km s^{-1}	Average, km s^{-1}	Median, km s^{-1}
1980	135	19–911	355	298
1984	43	28–346	157	123
1985	39	50–1280	458	235
1986	62	42–934	371	285
1987	118	42–671	262	236
1988	241	36–814	322	263
1989	298	50–944	410	357

from 1985 is 458 km s^{-1}, the highest value for any year of SMM observations. Among the other annual distributions of Figure 3, that for 1987 shows the tendency for many slow but few fast ejections (and a low average speed of 262 km s^{-1}), while that for 1989 shows the occurrence of many fast ejections (and a high average speed of 410 km s^{-1}). A similar result is found for the class of "outer loops" introduced above. The familiar set of statistical parameters for the speeds of outer loops measured during each calendar of SMM operations are listed in Table 3 (with the 5th to 95th percentile range given only for years with 32 or more measurements). These parameters indicate the paucity of low speed outer loops for every year and similar changes in the annual distributions.

Two possible "sampling effects" should be considered in assessing the reality of the changes in annual speed distributions and statistical parameters. The first of these stems from the smaller numbers of ejections observed during 1984 and 1985 (when the rate of occurrence of mass ejections was low); could the changes in the distributions and statistical parameters stem from the poor sampling of an unchanging statistical distribution (close to the "all-time" distribution of Figure 1) for those years? We believe this to be unlikely because the 1984 and 1985 average speeds differ from the all-time average by substantial fractions of the standard deviation (about the average) in the all-time distribution. Specifically, the standard deviation about the average for the distribution of Figure 1 is 289 km s^{-1}. The deviations in the 1984 and 1985 average speeds from the "all-time" average are −192 and +109 km s^{-1}. The magnitudes of these deviations are thus 0.66 and 0.38 of the standard deviations about the averages for the entire epoch. Such deviations are not likely to be the result of poor sampling.

The second of these sampling effects stems from the fact

Table 3. Statistical Parameters of the Annual Speed Distributions for Outer Loops

	No.	Range, km s^{-1}	Average, km s^{-1}	Median, km s^{-1}
1980	44	22–1097	457	367
1984	9	...	130	88
1985	14	...	574	329
1986	24	...	475	399
1987	32	79–669	329	312
1988	83	97–984	426	364
1989	125	81–1055	486	441

that a speed measurement is possible only if a mass ejection feature is seen on more than one coronagraph image. As with most spacecraft systems, the SMM coronagraph obtained images in a regular temporal sequence during the daylight portions of its orbit around the earth. The probability that an outward moving feature is seen within the coronagraph field of view is obviously smaller for faster moving features (as in the work by *Hundhausen et al.* [1984]); fast moving mass ejections will be underrepresented in any set of observations or measurements such as that under discussion here. Further, the temporal sequence of SMM observations was different in 1980, in 1984–1986 and (after a failure of an on-board tape recorder) in 1987–1989. The importance of this sampling effect on the distribution and statistics of observed speeds can be estimated by noting the annual fractions of mass ejections that were observed in a single image, presumably because of high outward speeds. This fraction was between 4% and 7% for all years between 1980 and 1988 except for 1984, when it was ~1%. That is, the fraction of observed mass ejections that moved so rapidly as to make speed measurements impossible did not change radically over that time period. This fraction was, however, ~13% for 1989. There may have been a significant change in the speed distribution toward higher speeds in 1989 that escaped detection by the SMM coronagraph.

Comparisons

Two other extensive sets of mass ejection speed measurements are available for comparison. *Gosling et al.* [1976] report an average speed of 470 km s^{-1} for the leading edges of 38 coronal mass ejections observed with the Skylab coronagraph in 1973–1974. The Skylab measurements included 26 speeds obtained in a manner similar to that used here and 12 lower limits to the speeds for those mass ejections seen in a single image. The Skylab average is distinctly higher than the SMM average for all features and comparable to the SMM average for outer loops. The comparison of Skylab and SMM measurements might be affected by the much shorter duration of the former, less than a full year. However, the Skylab average speed is higher than any annual SMM average for all features and higher than four of the seven annual SMM averages for outer loops. The comparison might be slightly affected by several differences in the analyses, correction for projection effects and inclusion of lower limits for some mass ejections observed by Skylab. Nonetheless, it seems evident that Skylab observed a group of 38 coronal mass ejections with higher speeds than the 673 ejections included in the SMM analysis.

Solwind coronagraph observations from 1979 to 1985 provide the largest set of speed determinations for comparison. *Howard et al.* [1985] show the distribution of speeds for the leading edges of 353 (R. A. Howard, private communication, 1993) mass ejections observed in 1979–1981. The average and median speeds derived from this distribution are approximately 470 and 200 km s^{-1}. The SMM observations from 1980 were made during a subset of this 1979–1981 epoch. Curiously, the Solwind average is higher than the 355 km s^{-1} SMM average value from 1980, but the Solwind median is lower than the 298 km s^{-1} SMM median value from 1980. *Howard et al.* [1986] show the speed distribution for 15 mass ejections observed between June 1, 1984, and May 1, 1985, and find an average speed of 208 km s^{-1}. The average speed of the ejections observed with the SMM coronagraph during this identical epoch is 169 km s^{-1}, comparable to but again lower than the Solwind value.

All of the comparisons suggest a systematic difference between the distributions of mass ejection speeds derived from SMM observations and those derived from Skylab and Solwind observations. In terms of average values for all reported speed measurements, this difference is 35% in comparison with Skylab and 32% and 23% in comparison with two different epochs of Solwind observations. Each of these comparisons is compromised by differences in measurement techniques or difficulties in finding large and comparable samples from the same or a comparable epoch. Further, the Solwind observations were made in an instrument field of view distinctly farther from the Sun than for SMM. The acceleration of mass ejections, summarized earlier could lead to a systematic difference. There is, however, no evidence here for a systematic difference by a factor of ~2 as found by *Hildner* [1986] on the basis of a very preliminary comparison of SMM and Solwind speed measurements.

Interpretation

Two aspects of the apparent speed distributions in Figures 1 and 2 invite comment. First, both distributions contain values lower than any solar wind speeds that have been observed in interplanetary space and the average values, ~350 km s^{-1} for all features and ~450 km s^{-1} for outer loops, are comparable to but less than the average solar wind speed of ~470 km s^{-1} [*Feldman et al.*, 1977]. Only a minority of the mass ejections observed in the 1.6 to 4–6 solar radii field of the SMM instrument are moving fast enough to overtake a normal interplanetary solar wind, especially with a sufficiently high differential speed to produce strong interplanetary shock waves. Unless there is a substantial additional acceleration of mass ejections beyond a heliocentric distance of 4–6 solar radii, many mass ejections will be accommodated into the solar wind without a strong compressive interaction at their leading edge (see also *Gosling et al.* [1976, 1991]). The slower mass ejections must be accelerated in being accommodated into the solar wind where speeds below ~250 km s^{-1} are rare.

A similar conclusion can be drawn regarding the interaction of mass ejections with the plasma in the region of the corona where the ejections are actually observed (and where the coronal expansion speed is expected to be substantially lower than its ultimate interplanetary value). *Hundhausen et al.* [1987] emphasized the comparison of mass ejection speeds with the local speeds of the two small-amplitude waves that can propagate outward along the nearly radial magnetic field. They estimated that near a heliocentric distance of 3 solar radii, the Alfvén speed is roughly 600 km s^{-1} and the sound speed is about 175 km s^{-1}. Figures 1 and 2 show that only a small fraction of the mass ejections observed in the SMM field were moving faster than the local Alfvén speed (about 20% of all features, 25% of outer loops). A comparable fraction (about 30% of all features, 15% of outer loops) were moving more slowly than the local sound speed. A majority of these ejections were moving at speeds between the local sound and Alfvén speeds. In overtaking the outward flowing coronal plasma, the majority of ejections could drive slow MHD shock waves as suggested by *Hundhausen et al.* [1987]. Among the annual speed distributions of Figure 3 there are no examples where the majority of

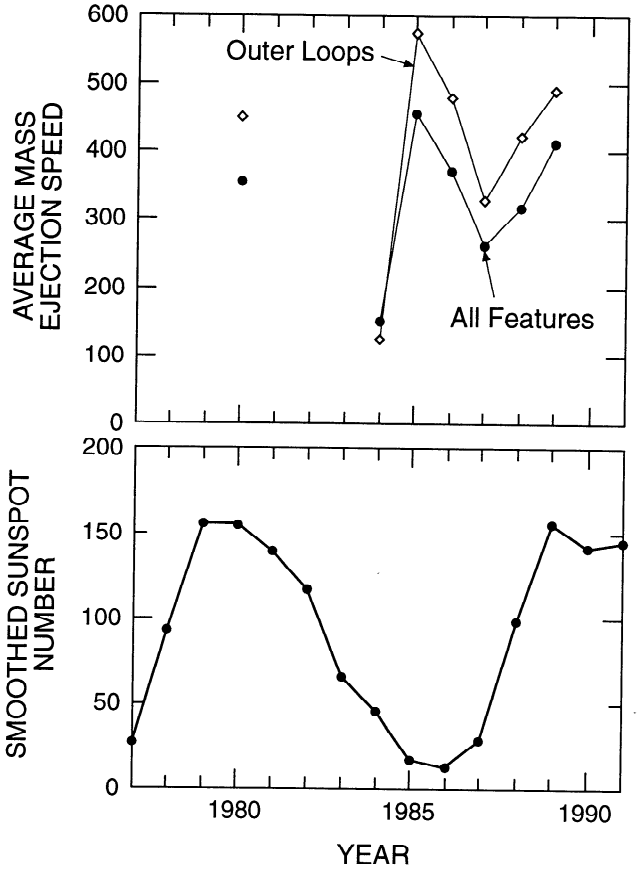

Figure 4. (top) The annual average speed values for all features (dots) and outer loops (diamonds) for the epoch of SMM observations and (bottom) the mean annual sunspot number from 1977 through 1991.

mass ejections moved faster than the Alfvén speed. In the extreme year of 1984, a majority of the observed mass ejections were moving subsonically. In all other years, most mass ejections moved outward through the SMM field of view supersonically but sub-Alfvénically.

The changes in the annual speed distributions of Figure 3 and the statistical quantities in Tables 2 and 3 raise the question of systematic variations in response to the solar activity cycle [e.g., *Hildner*, 1977; *Hundhausen et al.*, 1984; *Sheeley et al.*, 1986; *Howard et al.*, 1985, 1986; *Webb*, 1991; *Webb and Jackson*, 1993]. In the earlier description of the widths and locations of mass ejections observed with the SMM instrument, *Hundhausen* [1993] found no evidence for any large or systematic variation in mass ejection angular widths. However, the spread of mass ejections about the solar equator did change systematically in a manner similar to that of bright features in the quiet corona. *Webb* [1993] has interpreted the same Solwind average speeds cited above for 1979–1980 and 1984–1985 as evidence for higher speeds near solar cycle maximum than at minimum.

Figure 4 shows the annual averages of mass ejection speeds for all features and for outer loops, along with the annual mean sunspot numbers for the same epoch. To the conventional degree that the sunspot number is an index of solar activity, Figure 4 does not suggest a systematic variation in mass ejection speeds in response to the activity cycle. Average speeds during the 2 years near the minimum in sunspot number, 1985 and 1986, are comparable to those in the years nearest the last two maxima in sunspot number, 1980 and 1989 (but with the possibility that the 1989 distribution has been affected by a poorer sampling of fast mass ejections). The 2 years with abnormally low average speeds, 1984 and 1987, came on the descending and ascending parts of the sunspot cycle. No simple relationship of mass ejections speeds to the level of solar activity is discernible in Figure 4. The conclusion of *Webb* [1993] is not confirmed by the more extensive SMM observations. The specious nature of any inference of cyclic variations based on measurements from two epochs shorter than the suggested cycle could hardly be better illustrated.

4. Relationships Among Mass Ejection Sizes, Locations, and Speeds

The availability of a large set of mass ejection size, location, and speed measurements permits a search for any relationships among these mass ejection properties. Consider then the three pairs of these properties, with angular widths and apparent latitudes taken from the most recent tabulation of *Burkepile and St. Cyr* [1993]. For most mass ejections, single values of width and location were measured, usually for the outer most visible feature. (The nearly radial propagation of most mass ejections and the nearly radial edges seen for most features imply that these properties do not depend strongly on the height at which they were measured.) The speed measurements for the same feature only are involved in the following analysis.

Speed and Latitude

Figure 5 displays as crosses the apparent speed (as the ordinate) and apparent latitude (as the abscissa) of the 661 mass ejections for which SMM measurements of both quan-

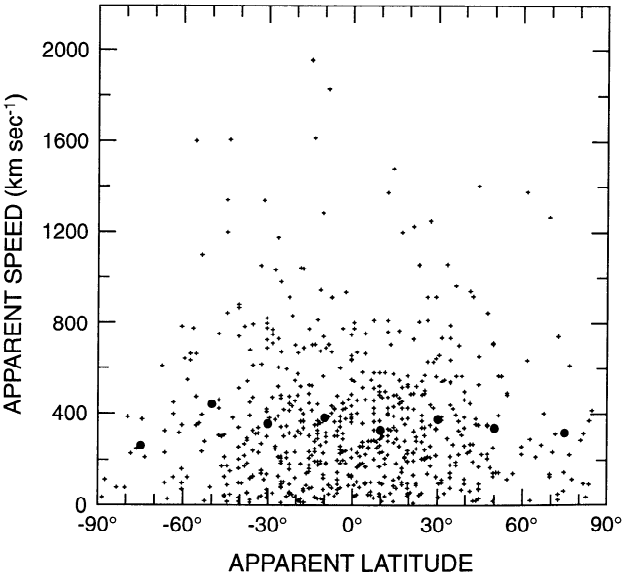

Figure 5. The apparent speed (as the ordinate) and apparent latitude (as the abscissa) for all 661 mass ejection features where both quantities were measured. The bold dots indicate the average speeds in 20° latitude intervals from −60° to +60° and in 30° intervals from −90° to −60° and 60° to 90°.

tities are available. The display is indeed a "scatter plot" with the crosses spread in a seemingly random manner throughout the ranges covered by both quantities. The average speeds in 20° intervals of latitude within 60° of the solar equator and a single 30° interval in each hemisphere beyond 60° are indicated by the large dots on Figure 5. These averages are nearly independent of latitude except in the very highest latitude intervals where the average speeds are slightly lower. This impression is reinforced by computation of the linear cross-correlation coefficient (as in the work by *Bevington* [1969]) between the speed and the absolute value of apparent latitude; the absolute value was chosen to detect any dependence of speed on latitude that is symmetric about the solar equator. For the 661 speed-latitude pairs of Figure 5, the cross-correlation coefficient is −0.029. The negative value confirms the small decrease in speed at high latitude suggested by the average values. The magnitude of ~0.03 demonstrates that the relationship between these two quantities is extremely weak.

Angular Width and Location

Figure 6 displays as crosses the apparent angular width (as the ordinate) and apparent latitude (as the abscissa) of the 1462 mass ejection features for which SMM measurements of both quantities are available (note that there are more measurements of width and location than of the speed). The average widths in the same latitude intervals used above are shown as large dots. The average angular widths of high-latitude mass ejections are slightly larger than the average widths at low latitudes; this may be a projection effect, as mentioned by *Hundhausen* [1993]. The cross-correlation coefficient between these angular widths and the absolute value of latitude is +0.133. This value confirms the increase in width with latitude and demonstrates that the relationship between these two quantities, while stronger than that between speed and latitude, is still weak.

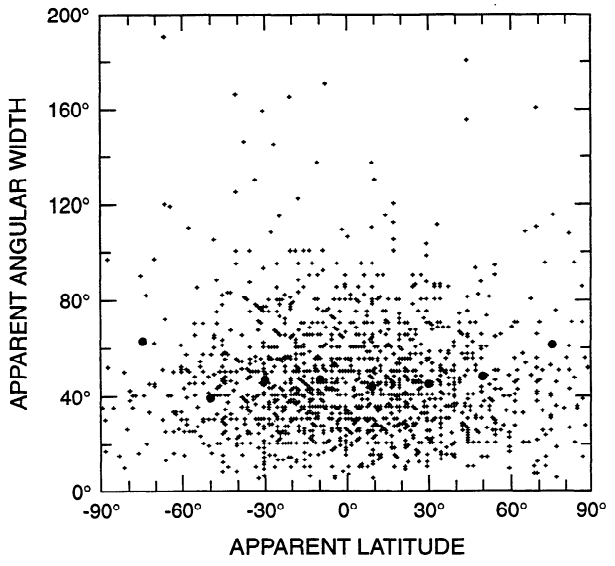

Figure 6. The apparent angular width (as the ordinate) and apparent latitude (as the abscissa) for all mass ejection features where both quantities were measured. The bold dots indicate the average widths in the same latitude intervals as Figure 5.

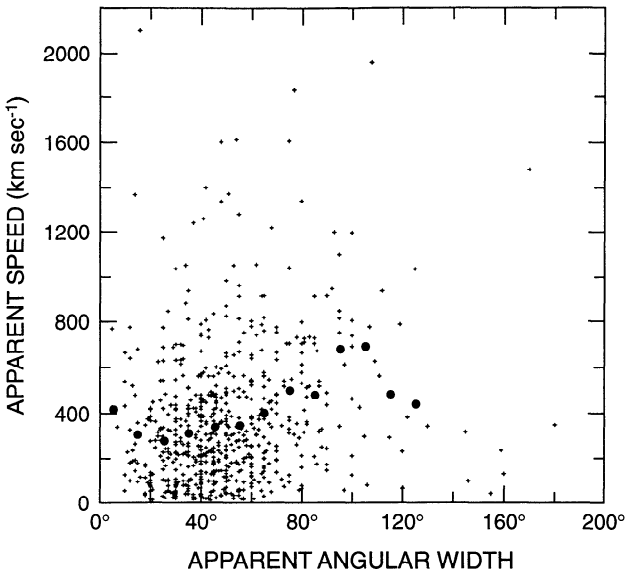

Figure 7. The apparent speed (as the ordinate) and apparent angular width (as the abscissa) for all mass ejection features for which both quantities were measured. The bold dots indicate the average speeds in 10° width intervals from 0° to 120° and in a single interval from 120° to 200°.

Speed and Angular Width

Finally, Figure 7 displays the apparent speed (as the ordinate) and apparent angular width (as the abscissa) of the 661 mass ejections for which SMM measurements of both quantities are available. The average speeds in 20° intervals of angular width are shown by the large dots on Figure 7. The average speeds are nearly constant for mass ejections of small or average width (near 40°) but higher for the few ejections with atypically large widths (above 60°). The cross-correlation coefficient between these speeds and angular widths is 0.210. This value confirms an increase in speed with increasing size but again demonstrates that the overall relationship is weak.

Interpretation

The scatter plots, average values, and cross-correlation coefficients described above all indicate that relationships among mass ejection width, latitude, and speed are weak. The strongest correlation indicates a positive relationship between mass ejection speed and angular width. A smaller correlation indicates a positive relationship between angular width and the absolute value of mass ejection latitude. The smallest cross-correlation coefficient indicates a very weak negative relationship between mass ejection speed and the absolute value of latitude.

The two latter relationships have interesting implications regarding the connection between coronal mass ejections and other forms of solar activity. *Hundhausen* [1993] showed that most high-latitude mass ejections occurred at epochs of high activity but well poleward of the active latitudes, i.e., the sites of such familiar, small-scale manifestations of activity as sunspots, active regions, or optical (Hα) flares. These high-latitude ejections did occur during the epoch when solar prominences and bright coronal features (such as coronal helmet streamers) migrated to high latitudes. This statistical relationship and the clear association

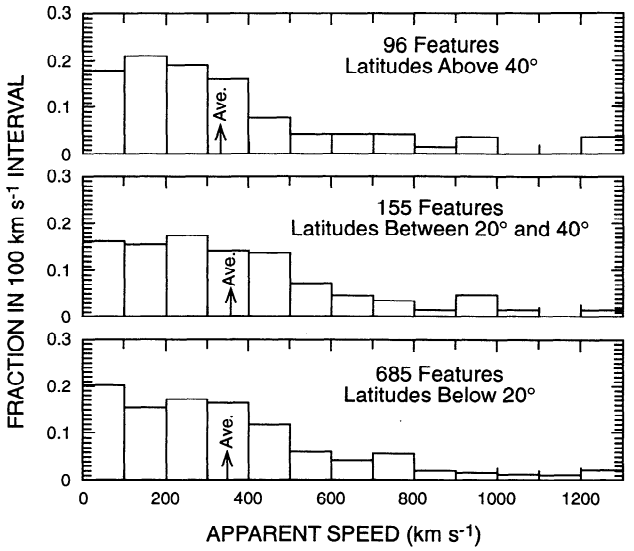

Figure 8. The apparent speed distributions of mass ejection features centered at high latitudes (above 60° in apparent heliographic latitude), active latitudes (between 20° and 40° in apparent latitude), and equatorial latitudes (within 20° of the heliographic equator). The average apparent speeds in each interval 332, 359, and 349 km s^{-1}, respectively, are indicated on each frame.

of many individual, high-latitude mass ejections with eruptions of high-latitude prominences suggested that the former were unrelated to solar activity on small spatial scales but were probably related to the evolution of large-scale magnetic and coronal structures. The correlations summarized above indicate that these high-latitude mass ejections are not a "weak" form of coronal activity. On the average, high-latitude coronal mass ejections are somewhat larger (in apparent angular width) and only slightly slower than their lower-latitude counterparts. This latter point is emphasized in Figure 8, a display of the distributions of the apparent speeds of mass ejection features in three separate latitude intervals. These intervals contain mass ejections within 20° of the solar equator, in the range 20° to 40° from the equator (the active latitudes at the epochs when most mass ejections were observed), and more than 40° from the equator (the latitudes polewards of small-scale activity). The 332 km s^{-1} average speed of the 96 high-latitude ejections is only slightly lower than the 359 km s^{-1} value for the 155 active latitude ejections. Further, the fraction of very fast ejections, with apparent speeds greater than 1200 km s^{-1}, is larger at the high latitudes than in the active latitudes.

5. Summary

We have presented here a statistical description of the apparent speeds of 936 coronal mass ejection features observed with the SMM coronagraph in 1980 and from 1984 through 1989. Along with the earlier description of the sizes and locations of these ejections [*Hundhausen*, 1993], this completes the exposition of the basic (and easily measured) mass ejection properties from the largest extant set of measurements. A similar analysis of the brightness and mass and energy contents of these ejections is underway.

The apparent speeds measured from the SMM data set are distributed over the range (defined by the 5th and 95th percentiles of the observed distribution) of 35 to 911 km s^{-1}. The average speed for all observed features is 349 km s^{-1}. This average is lower (by ~30%) than the average speeds reported from less extensive Skylab and Solwind observations. The significance of this difference is not clear in light of differences in analysis techniques and fields of view and of the difficulty in finding comparable samples of mass ejections. The speed distribution for all features, outermost features, and most prominent features in each ejection are little different. However, the speed distributions for different mass ejection "morphologies" do differ. In particular, the outer loops seen in 47% of all SMM mass ejections move with higher speeds. The speed distribution for outer loops ranges from 80 to 1042 km s^{-1} and has an average speed of 445 km s^{-1}.

The annual distributions of mass ejection speeds from the SMM epoch reveal significant changes. This variability is epitomized by the distributions for two consecutive years, 1984 and 1985. In 1984, no mass ejections were observed with speeds greater than 420 km s^{-1}, and the average speed was only 157 km s^{-1}. In 1985, 38% of the observed mass ejections had speeds greater than 400 km s^{-1}, and the average speed of 458 km s^{-1} exceeded the highest speed seen in 1984. There is, however, no evidence here that these changes reflect the solar activity cycle. The average speeds for the 2 years near sunspot minimum (1985 and 1986) are comparable to those for the 2 years nearest sunspot maxima (1980 and 1989).

Finally, the three mass ejection properties described here and by *Hundhausen* [1993] are only weakly related. The high-latitude ejections identified in that earlier work as occurring well poleward of the "active latitudes" (defined by small-scale activity such as sunspots, active regions, or optical flares) have an average angular width that is slightly larger than that for ejections from active or equatorial latitudes. The average speed of these high-latitude ejections is only slightly lower than for active latitude ejections.

Appendix: Projection of Mass Ejection Speeds

The radiation recorded on the SMM coronal images used here is a portion of the photospheric radiation scattered by electrons in the corona. Since the corona is optically thin in this radiation, virtually all of the light scattered along a given line of sight through the corona is detected as though coming from a point on an image plane or, more accurately, on the "plane of the sky" defined as the plane passing through the center of the Sun and normal to the "Sun-observer line." This light is thus attributed to a heliocentric distance equal to the "impact parameter" of the line of sight. This geometry, the intensity of scattering along the line of sight, and the implication of projection upon the plane of the sky regarding the observed locations of mass ejections were discussed by *Hundhausen* [1993].

The effect of this same projection on the observed or apparent speeds of mass ejections is easily quantified for a "narrow" ejection. If a narrow spike of high-density plasma were to move radially out through the corona (as sketched in the top panel of Figure 9) at an angle θ out of the plane of the sky, the apparent or projected heliocentric position R of the top of the spike is the simple projection

$$R = r \cos \theta$$

of its true heliocentric position r. Hence its apparent speed v_{app} measured from a time sequence of images would be related to its true speed v by

$$v_{app} = \frac{dR}{dt} = \cos\theta \frac{dr}{dt} = v \cos\theta$$

This simple trigonometric projection factor was used, for example, by *Gosling et al.* [1976] to deduce the true speeds of some mass ejections observed with the Skylab coronagraph.

A majority of the mass ejection features observed with the SMM instrument have a curved front (classified as loops, mounds, or clouds by *Burkepile and St. Cyr* [1993]). The projection of speeds for such features is easily estimated if the front of the ejection is idealized as a spherical region of dense plasma whose center moved radially out through the corona (as sketched in the bottom panel of Figure 9; see also *Fisher and Munro* [1984] and *Eselevich and Filippov* [1991]) at an angle θ out of the plane of the sky. The apparent bright front or leading edge of the mass ejection would be seen on an image at the apparent or projected heliocentric distance

$$R = r_c \cos\theta + \rho$$

where r_c is the heliocentric position of the center of the sphere and ρ is the radius of the spherical front. The apparent speed v_{app} of the front measured from a time sequence of images would be

$$v_{app} = \frac{dR}{dt} = \frac{dr_c}{dt} \cos\theta + \frac{d\rho}{dt}$$

Most mass ejections observed with the SMM coronagraph maintain a nearly constant angular size as they move through the instrumental field of view. Hence it is reasonable to assume here that

$$\frac{\rho}{r_c} = \sin\frac{\omega}{2}$$

where ω is the angle about the Sun center subtended by the spherical region of dense plasma. Thus ω corresponds to the angular width of the mass ejection. Then

$$v_{app} = \left(\cos\theta + \sin\frac{\omega}{2}\right)\frac{dr_c}{dt}$$

The top of the dense region is moving radially outward at the true speed

$$v = \frac{d}{dt}(r_c + \rho) = \left(1 + \sin\frac{\omega}{2}\right)\frac{dr_c}{dt}$$

Hence the apparent and true speeds are related by

$$\frac{v_{app}}{v} = \frac{\cos\theta + \sin(\omega/2)}{1 + \sin(\omega/2)}$$

Figure 10 is a plot of this ratio as a function of the angle of the mass ejection center from the plane of the sky, for ω =

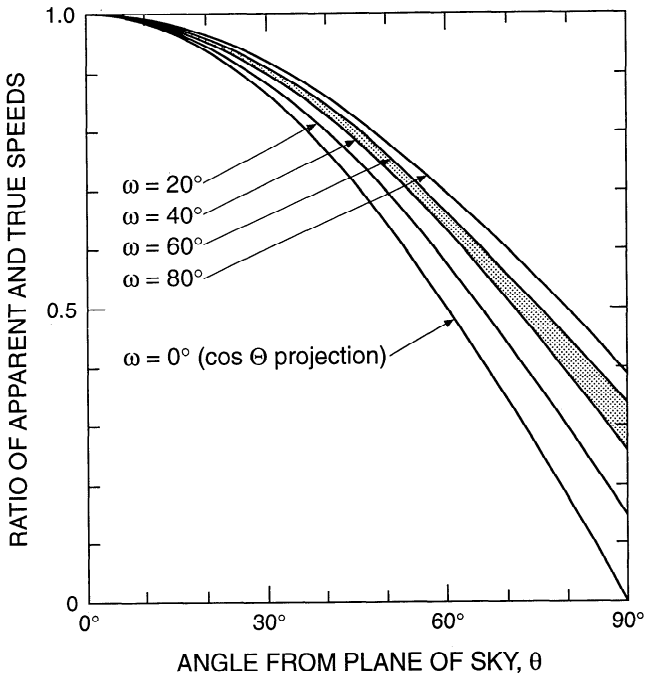

Figure 10. The ratio of apparent or projected speed to the true speed as a function of angle away from the plane of the sky for spherical fronts with angular sizes from 0° to 80°. Typical mass ejection angular widths are in the 40° to 60° range, shaded on the figure.

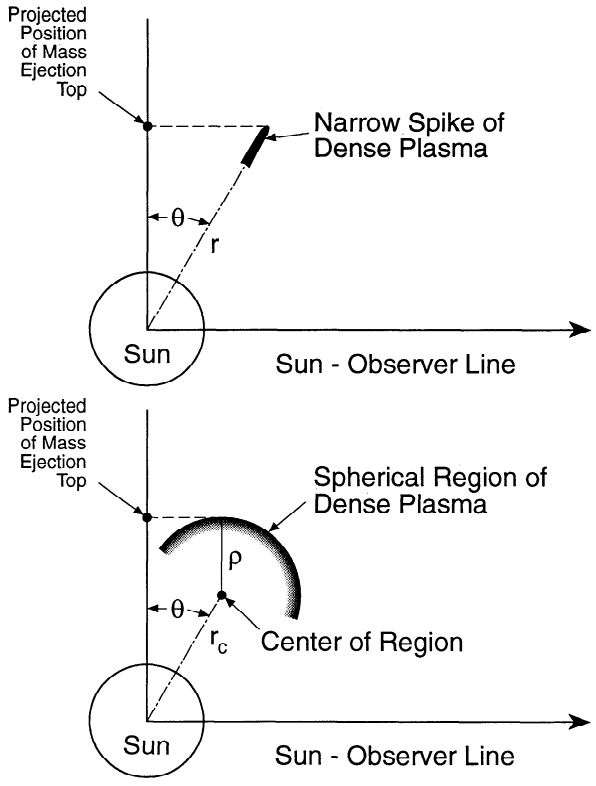

Figure 9. (top) The projection of a narrow spike of dense plasma and (bottom) the front of a spherical region of dense plasma onto the plane of the sky. Each drawing is in a plane defined by the observer, the center of the sun, and either the axis of the spike (top) or center of the spherical region (bottom). The angle θ gives the displacement of the axis of each structure from the plane of the sky.

0°, 20°, 40°, 60°, and 80°. The average angular widths of mass ejections observed with the SMM instrument are 46° for all features and 55° for outer loops; thus the typical ejection would fall in the shaded band between the 40° and 60° curves on Figure 10. The effect of projection on the speeds of mass ejection features with bright curved fronts is smaller than the trigonometric, cosine factor. For features of typical angular size seen within 35° of the solar limb [see *Hundhausen*, 1993], the correction for this effect is always less than 13%.

Acknowledgments. The authors acknowledge discussions with and comments by D. F. Webb and D. G. Sime on the material in this paper. The National Center for Atmospheric Research is sponsored by the National Science Foundation. The SMM observations and analysis reported here were funded under NASA contract S-04167D. We would also like to thank Liz Boyd for preparing this manuscript.

The Editor thanks J. T. Gosling and an other referee for their assistance in evaluating this paper.

References

Bevington, P. R., *Data Reduction and Error Analysis for the Physical Sciences*, McGraw-Hill, New York, 1969.

Burkepile, J. T., and O. C. St. Cyr, A revised and expanded catalogue of mass ejections observed by the Solar Maximum Mission coronagraph, *NCAR Tech. Note NCAR/TN-369+STR*, Natl. Cent. for Atmos. Res., Boulder, Colo., 1993.

Eselevich, V. G., and M. A. Filippov, On the dynamic and structure of coronal mass ejections, *Planet. Space Sci.*, *39*, 737–744, 1991.

Feldman, W. C., J. R. Asbridge, S. J. Bame, and J. T. Gosling, Plasma and magnetic fields from the Sun, in *The Solar Output and Its Variation*, edited by O. R. White, pp. 351–381, Colorado Associated University Press, Boulder, 1977.

Fisher, R. R., and R. H. Munro, Coronal transient geometry, 1, The flare-associated event of 1981 March 25, *Astrophys. J.*, *280*, 428–439, 1984.

Gosling, J. T., E. Hildner, R. M. MacQueen, R. H. Munro, A. I. Poland, and C. L. Ross, The speeds of coronal mass ejection events, *Sol. Phys.*, *48*, 389–397, 1976.

Gosling, J. T., D. J. McComas, J. L. Philips, and S. J. Bame, Geomagnetic activity associated with Earth passage of interplanetary shock disturbances and coronal mass ejections, *J. Geophys. Res.*, *96*, 7831–7839, 1991.

Hildner, E., Mass ejections from the corona into interplanetary space, in *Study of Travelling Interplanetary Phenomena*, edited by M. A. Shea, D. F. Smart, and S. T. Wu, pp. 3–21, D. Reidel, Norwell, Mass., 1977.

Hildner, E., Do we understand coronal mass ejections yet?, *Adv. Space Res.*, *6*(6), 297–306, 1986.

Howard, R. A., N. R. Sheeley, Jr., M. J. Koomen, and D. J. Michels, Coronal mass ejections, 1979–1981, *J. Geophys. Res.*, *90*, 8173–8191, 1985.

Howard, R. A., N. R. Sheeley, Jr., M. J. Koomen, and D. J. Michels, The solar cycle dependence of coronal mass ejections, in *The Sun and the Heliosphere in Three Dimensions*, edited by R. G. Marsden, p. 107–111, D. Reidel, Norwell, Mass., 1986.

Hundhausen, A. J., Sizes and locations of coronal mass ejections: SMM observations from 1980 and 1984–1989, *J. Geophys. Res.*, *98*, 13,177–13,200, 1993.

Hundhausen, A. J., C. B. Sawyer, L. House, R. M. E. Illing, and W. J. Wagner, Coronal mass ejections observed during the Solar Maximum Mission: Latitude distribution and rate of occurrence, *J. Geophys. Res.*, *89*, 2639–2646, 1984.

Hundhausen, A. J., T. E. Holzer, and B. C. Low, Do slow shocks precede some coronal mass ejections?, *J. Geophys. Res.*, *92*, 11,173–11,178, 1987.

MacQueen, R. M., Coronal transients: A summary, *Philos. Trans. R. Soc. London, Ser. A*, *297*, 605–620, 1980.

Munro, R. H., and D. G. Sime, White light coronal transients observed from Skylab, May 1973 to February 1974: A classification by apparent morphology, *Sol. Phys.*, *97*, 191–201, 1985.

Sheeley, N. R., Jr., R. A. Howard, M. J. Koomen, and D. J. Michels, Solwind observations of coronal mass ejections during 1979–1985, in Solar Flares and Coronal Physics Using P/OF as a Research Tool, edited by E. Tandberg-Hanssen, R. M. Wilson, and H. S. Hudson, *NASA Conf. Publ.*, *2421*, 241–256, 1986.

St. Cyr, O. C., and J. T. Burkepile, A catalogue of mass ejections observed by the Solar Maximum Mission coronagraph, *NCAR Tech. Note NCAR/TN-352+STR*, Natl. Cent. for Atmos. Res., Boulder, Colo., 1990.

Webb, D. F., The solar cycle variation of the rates of CMEs and related activity, *Adv. Space Res.*, *11*(1), 37–40, 1991.

Webb, D. F., The heliospheric manifestations and geoeffectiveness of solar mass ejections, in *Solar-Terrestrial Predictions Workshop: IV*, National Oceanic and Atmospheric Administration, Boulder, Colo., in press, 1993.

Webb, D. F., and B. V. Jackson, Characteristics of CMEs observed in the heliosphere using Helios photometer and in-situ data, in *Solar-Terrestrial Predictions Workshop: IV*, National Oceanic and Atmospheric Administration, Boulder, Colo., in press, 1993.

J. T. Burkepile and A. J. Hundhausen, High Altitude Observatory, NCAR, P.O. Box 3000, MS 2920, Boulder, CO 80303-3000.

O. C. St. Cyr, AlliedSignal Technical Services Corp., Code 682, NASA Goddard Space Flight Center, Greenbelt, MD 20770.

(Received July 13, 1993; revised November 15, 1993;
accepted December 16, 1993.)